



ELSEVIER

Available online at www.sciencedirect.com

SCIENCE @ DIRECT®

Ocean Engineering 32 (2005) 1404–1419

OCEAN
ENGINEERING

www.elsevier.com/locate/oceaneng

Analysis of sea waves and wind from X-band radar

P. Izquierdo, C. Guedes Soares*

*Unit of Marine Technology and Engineering, Technical University of Lisbon, Instituto Superior Técnico,
Av. Rovisco Pais, 1049-001 Lisboa, Portugal*

Received 20 August 2004; accepted 19 November 2004

Available online 9 March 2005

Abstract

This paper presents the results of a calibration study aimed at verifying the adequacy of a system to analyse images from a X-band radar in order to measure the ocean waves and wind fields. Spectral analysis of the time series of radar images is performed to determine directional spectra of the ocean wave fields and also their spectral parameters. The radar is calibrated to measure ocean waves and the results of a comparison with a directional waverider buoy located in an area close to the port are presented, evaluating the performance of the system as concerns the determination of sea-state parameters and directional spectra. A preliminary study of the capability of this radar system to estimate wind fields is also presented, showing the calibration results with measured wind fields for different directional sectors.

© 2005 Elsevier Ltd. All rights reserved.

Keywords: Ocean waves; Directional spectra; Sea-state parameters; Wind speed and X-band radar

1. Introduction

Typical X-band nautical radars are being used to monitor current and ocean waves, providing the ocean wave directional spectrum and different sea state parameters (Heathershaw et al., 1980; Nieto Borge et al., 1999). These radars operate by transmitting an electromagnetic field that interacts with the roughness of the sea surface and receiving the backscatter of this field. The backscattered signal is composed of the speckle due to

* Corresponding author.

E-mail address: guedess@mar.ist.utl.pt (C. Guedes Soares).

the roughness associated with the ocean wind and the modulation produced by the surface gravity waves. The signal received by the radar is digitalised and recorded in time series of sea surface images.

The modulation of the backscatter pattern with the ocean waves can be used to describe the ocean wave fields in terms of its directional spectrum. The measurement of ocean waves and surface currents with X-band radar is based on the spatial and temporal structure analysis of radar images of the sea surface. The spectral analysis of image time series is used to retrieve the ocean wave directional spectrum and from this the sea-spectral parameters (Nieto Borge and Guedes Soares, 2000; Izquierdo et al., 2002; Izquierdo et al., 2004).

The image of the sea surface has a strong dependence on the wind (Hatten et al., 1998a), which makes it possible for the ocean wind fields to be retrieved from radar images sequences (Dankert et al., 2002). The local wind fields generate the small-scale roughness of the sea surface, raising the variance of the mean image intensity. So the image intensity depends on the wind speed and on the azimuth angle between the antenna viewing direction and the wind direction (Hatten et al., 1998b). Due to this dependence the nautical X-band radars can be used as a wind sensor, after a calibration is performed.

Some comparisons of wave spectra and sea-state parameters from nautical radar image time series and wave buoy data have been shown by Alfonso et al. (1997), Nieto Borge and Guedes Soares (2000) and by Izquierdo et al. (2002). A more systematic study has been made by Izquierdo and Guedes, 2004, who have made systematic comparisons of the sea-state parameters from a radar system and a scalar buoy, determining the statistics of the differences, and showing the effect on statistics of different methods of spectral estimation.

The present work is a follow-up of the later, by evaluating the performance of the X-band radar with reference to a directional waverider buoy and thus to analyse the directional capabilities of this systems to measure ocean wave fields. First results are also presented of the system performance to measure wind at the surface. The results of the calibration of the radar system with wind speeds measured at a meteorological station are shown, demonstrating that this system can also be useful to provide such information.

2. Ocean wave spectrum retrieval

The estimation of the ocean wave spectrum from a radar image time series, $\psi(\vec{r}, t)$, is accomplished by applying an inverse modelling technique (Nieto Borge and Guedes Soares, 2000) consisting in the following steps:

Image normalisation: Subtracting the temporal and spatial mean image intensity.

Spectrum estimation: Application of a three-dimensional discrete Fourier transform algorithm (3D-DFT) to obtain the discrete estimation of the three-dimensional image spectrum, $F_\psi(k, \omega)$ (Young et al., 1985).

Calculation of the surface current: The current is estimated by minimising a cost function, which depends on the square distance of the fitting points (k, ω) to the dispersion relation shell (Senet et al., 1997).

Filtering of the image spectrum: All energy that is not due to the wave field is removed from the image spectrum (Young et al., 1985).

Application of the image transfer function: This function connects the image spectrum values with the surface wave spectrum values (Nieto Borge et al., 1999).

The three-dimensional spectrum of ocean waves, $F_w(\vec{k}, \omega)$, is the output of this inverse method. Other more condensed spectral representations can be obtained by integration or transformation of wave coordinates, assuming the linear gravity wave dispersion relation.

The spectral densities, obtained by the described inversion method, have values that are related to the scale of sampled grey levels of the radar images, containing only relative information about the energy distribution of the wave field. Hence, the non-scaled spectrum cannot provide the variance of the sea surface elevation nor the related sea-state parameters such as the significant wave height. Therefore, to obtain the real spectral values corresponding to the sea state, each radar station needs to be calibrated with some other ocean wave sensor.

The radar calibration is based on a method developed for the synthetic aperture radar (Alpers and Hasselmann, 1982). The method is based on the assumption that the square-root of measured signal to noise ratio, SNR, is linearly related to significant wave height, H_S ,

$$H_S = A + B\sqrt{\text{SNR}} \quad (1)$$

where A and B are empirical parameters that have to be determined for each radar. The success of this method for deep-water applications has been shown by various authors (e.g. Nieto Borge et al., 1999).

3. Wind speed retrieval

The wind direction in the sea surface can be estimated from a time series of radar images by taking into account the dependence of the signal received on the azimuth angle between the antenna viewing direction and the wind direction (Hatten et al., 1998b; Dankert et al., 2002). The antenna look direction, for which the radar backscattering is maximum corresponds to the upwind direction. In comparison with other radars, the directional ambiguity in 180° does not occur for X-band radars, existing only one maximum in the upwind direction.

By applying a 3D-FFT algorithm to the time series of radar images, $\psi(\vec{r}, t)$, this is transformed to three-dimensional frequency-wavenumber domain, $F_\psi(\vec{k}, \omega)$. In the spectral domain, the speckle results in the background noise, $F_n(\vec{k}, \omega)$, and the modulation in the ocean wave signal, $F_w(\vec{k}, \omega)$. These two components can be separated by the dispersion relation of linear gravity waves, which is used as a filter in the analysis of ocean wave fields (Nieto Borge and Guedes Soares, 2000). The total variance of the spectral background noise can be used to estimate the ocean wind speed (Hatten et al., 1998a,b).

Nautical radars can be used as a wind sensor after a calibration with independent wind measurements. The dependence of the spectral noise, $F_n(\vec{k}, \omega)$, on the wind speed, V , is approximated with the following straight line

$$\sum_{\vec{k}, \omega} F_n(\vec{k}, \omega) = a + bV \quad (2)$$

The coefficients a and b are obtained by a linear regression fit for every angle class in which the image area has been divided. The ratio a/b is the minimum value of wind speed that the radar is capable of detecting. The fitted values of a and b in the wind direction is used to estimate the wind speed with the background noise of the image time series.

4. Data description

The data used in this work were collected close to the Port of Sines in Portugal, from September 2000 to December 2001, from an X-band radar system, a directional Datawell buoy and a meteorological station. In Fig. 1 it can be seen the locations of the different sensors in Cape of Sines.

The port of Sines traffic radar was used in this work to record image time series of the sea surface. The WaMoS system is a hardware and software system that captures the radar images which was used to record time series of consecutive polar radar images (Nieto Borge et al., 1999). In order to prepare the radar data for wave analysis, from each polar image a rectangular sub-area was chosen, and in this case its centre was positioned 255° in respect to north direction. For the present work, 32 consecutive images of 128×256 pixels were taken from the sub-area. The resolutions were 2.56 s in time, equal to the antenna revolution, and 4.88 m per pixel in space being the sub-area of $625 \times 1250 \text{ m}^2$ squared.

To calibrate the radar in order to estimate the real values of wave spectra, a directional waverider buoy, located close to the port, was used to record time series of heave-pitch-roll values. The buoy data were recorded every three hours and they consisted of 2304 heave-pitch-roll measurements with a time resolution of 0.78 s during a period of 30 min. The measurements consisted of 71 simultaneous series records from the radar and from the buoy during the experiment period.

A meteorological station, located in the same place of the radar in the Port of Sines, was used to evaluate the development of the wind measurement capability of the radar system.

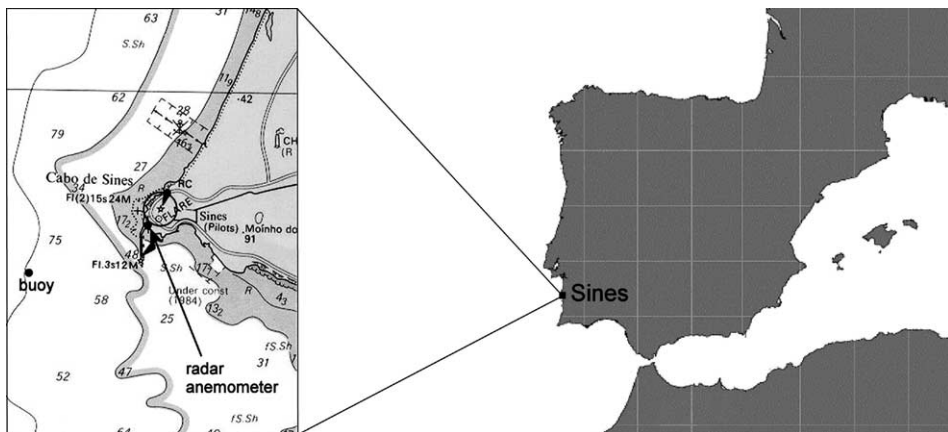


Fig. 1. Locations of different sensors in the Cape of Sines.

For this purpose, 925 simultaneous records of image time series from the radar and wind speed and direction from meteorological station were taken every 10 min.

5. Ocean wave spectra

The series of radar images were analysed to estimate the scalar and directional spectra, $S(f)$ and $E(f, \theta)$, with a maximum frequency of 0.35 Hz, solving the aliasing effect, (Seeman et al., 1997) and with 4° of freedom (d.o.f.). The sea surface spectra using series from the directional buoy were estimated through the cross-spectra by means of a 1D-DFT method (Longuet-Higgins et al., 1963) and the spectra were smoothed by Daniell's method with 30 d.o.f.

The calibration of Sines' radar was performed with a set of 444 simultaneous observations of signal to noise ratio SNR, estimated by the radar system, versus the significant wave height H_s , estimated by the buoy (Izquierdo et al., 2002). The parameters of the calibration were calculated by least-square fit of the estimations of both sensors and they are shown in the Fig. 2. After the calibration period, the real values of the ocean wave spectra can be estimated and, from these, the wave parameters that characterize the sea state.

In most of the analysed cases the buoy and the radar measured swells coming from northwest, typical in this costal area of the Atlantic Ocean. Fig. 3 shows an example of these scalar, (a), and directional (b), spectra, estimated from radar and buoy data.

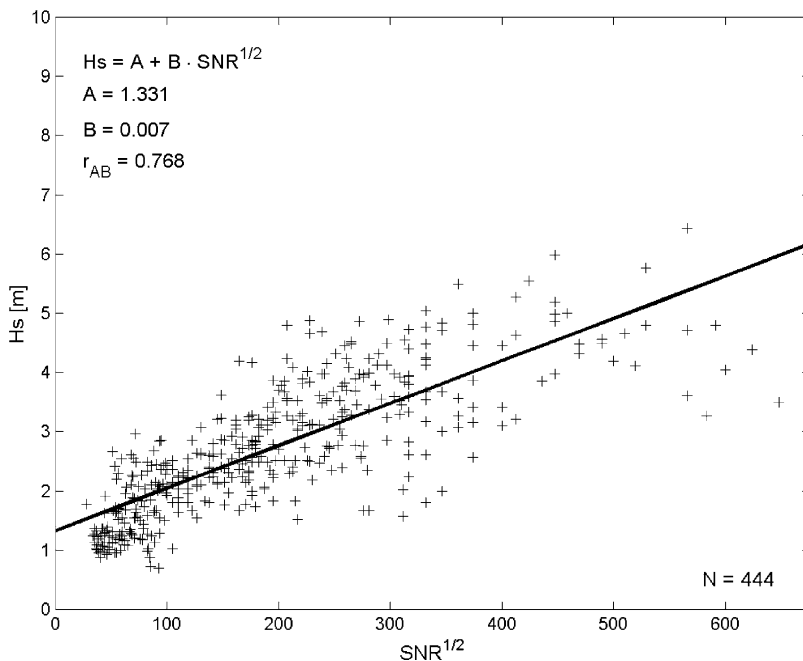


Fig. 2. Least-square fit to obtain the calibration parameters, A and B , of the Sines' radar (Izquierdo et al., 2002).

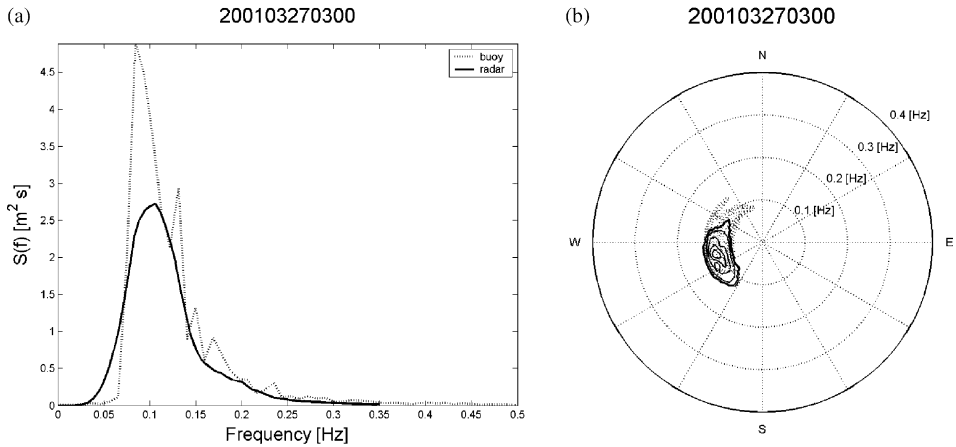


Fig. 3. (a) Frequency spectra from the radar (continuous line) and the buoy (dashed line), and (b) spectra in frequency and direction from the radar (continuous contour lines) and the buoy (dashed contour lines).

The shape of the scalar spectra, $S(f)$, measured by the radar is smoother than the estimates obtained from buoy data. This is due to two causes (Izquierdo et al., 2004), the first being that the frequency resolution of the radar is smaller than that of the buoy. The second and most important cause is that the spectrum $S(f)$ estimated by the radar is obtained from the integration in wave number of the 3-dimensional spectrum $F(\vec{k}, \omega)$. Because of this, the estimation that is obtained for $S(f)$ contains temporal and spatial information of the wave field, while for case of the buoy only temporal information at a given point is taken into account. Considering ocean waves as an ergodic process, the scalar spectrum obtained from radar image series is equivalent to that of a buoy smoothed with more degrees of freedom.

The directional spectra estimated by the radar show less dispersion in direction and more in frequency than those estimated by the buoy. This is due to buoy data having less directional resolution, the opposite to what happens with frequency resolution. In most cases, radar spectra were measured slightly more to the south than those of the buoy. Due to wave diffraction by the coastal line although the radar and the buoy were measuring in zones of close proximity, the spectra are nonetheless different (Fig. 1). The radar was measuring in a zone closer to the coast and the buoy was located more to southwest, where it may measure the wave field with less influence from the coast.

6. Sea state parameters

To evaluate the performance of the ocean wave spectral analysis of this radar, different sea-state parameters were estimated from spectra and they were compared with the simultaneous estimations from buoy spectra. The parameters used for this aim were significant wave height, H_s , peak frequency, f_p , mean period, T , spectral maximum, $\max\{S(f)\}$, spectral bandwidth, ν , and mean direction, θ .

Table 1

Mean and standard deviation values of the difference of sea-state parameters

	Mean	rms
H_S (buoy) – H_S (radar)	–0.08	0.53
f_p (buoy) – f_p (radar)	0.02	0.04
T (buoy) – T (radar)	–1.76	1.33
Max $\{S(f)\}$ (buoy) – max $\{S(f)\}$ (radar)	1.83	4.47
ν (buoy) – ν (radar)	0.08	0.09
θ (buoy) – θ (radar)	–25.16	16.01

The differences and ratios of the values of those parameters from buoy and radar spectra were also estimated. The mean and standard deviation of the differences and ratios were calculated and the values are given in Tables 1 and 2, respectively. From the results shown in these tables, it can be seen that H_S , f_p and ν had in general similar values from radar and buoy spectra, whereas max $\{S(f)\}$ and θ had different values from estimations of both sensors. The main differences between the sea-state parameters derived by using spectra obtained from both sensors result both from device characteristics (Izquierdo et al., 2004). The results of sea-state parameters are explained in more detail below.

6.1. Significant wave height

The significant wave height H_S had values between 1.5 and 3.5 m from radar estimations and between 0.5 and 4.5 m from buoy estimations. The time series of H_S values from radar and buoy spectra are given in Fig. 4. The radar series was smoother than the buoy series because radar spectra contain spatial and directional information while buoy spectra only contains temporal, as was explained in the previous section. In general, the values of the significant wave height estimated from radar and buoy data presented similar behaviour. The time series of this parameter of the radar had an evolution smoother than those of the buoy due to the fact that the estimation procedure of this parameter from radar data integrates spatial and time information while in the case of the buoy only temporal information is considered (Izquierdo et al., 2004).

6.2. Peak frequency

The peak frequency, f_p , was estimated by Delft's method defined by the IAHR working group (IAHR, 1989). This parameter derived from both sensors had similar values with

Table 2

Mean and standard deviation values of the ratio of sea-state parameters

	Mean	rms
H_S (buoy)/ H_S (radar)	0.95	0.28
f_p (buoy)/ f_p (radar)	1.15	0.37
T (buoy)/ T (radar)	0.77	0.17
max $\{S(f)\}$ (buoy)/max $\{S(f)\}$ (radar)	1.63	1.43
ν (buoy)/ ν (radar)	1.20	0.22
θ (buoy)/ θ (radar)	0.86	0.08

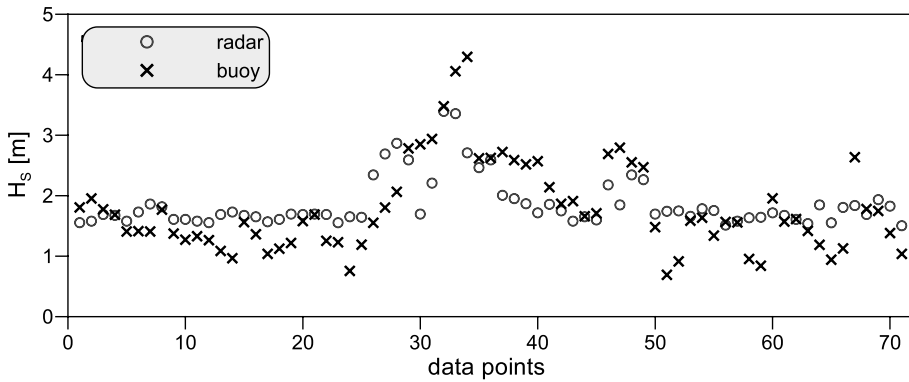


Fig. 4. Values of significant wave height estimated from radar and buoy spectra.

means of their differences and ratios very close to 0 and 1 Hz, respectively. The time series of f_p values from radar and buoy spectra are given in Fig. 5. The values of this parameter estimated from radar spectra were around 0.1 Hz because there were swells in most measurements. Except for some estimation for which the buoy gives higher values than the radar, they are around the same value from both sensors. The discrepancies between the values estimated from both sensors were due to the very small wind intensity, resulting in radar spectra with noise energy in low frequencies and located at frequencies lower than buoy.

6.3. Mean period

The mean period, \bar{T} , had values between 6 and 10 s from radar estimations and between 4 and 8 s from buoy estimations. The time series of simultaneous values of \bar{T} estimated from radar and buoy spectra are show in Fig. 6. The estimations from buoy spectra were lower in most of the cases. This is due to the dependence of this parameter on the spectral moment of second order, bearing in mind that the spectral moments of higher order

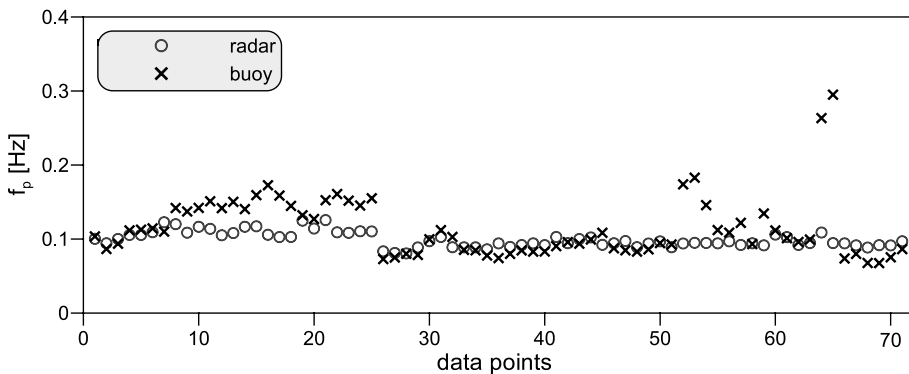


Fig. 5. Values of peak frequency estimated from radar and buoy spectra.

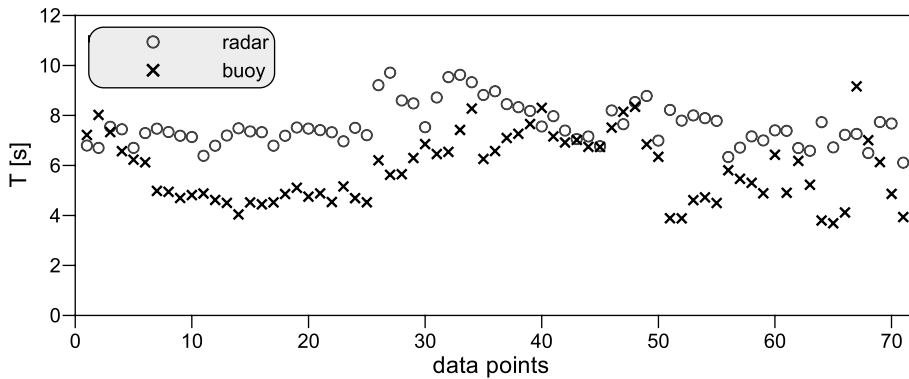


Fig. 6. Values of mean period estimated from radar and buoy spectra.

enhance the effect of spectral energy at high frequencies (Izquierdo et al., 2004). The maximum frequency of radar spectra (0.35 Hz) is lower than the one of buoy spectra (0.65 Hz), the energy of buoy spectra located at frequencies higher than maximum frequency of the radar is resulting in an underestimation of this parameter from the buoy spectra, in comparison with the mean period estimation from the radar spectra.

6.4. Spectral maximum

The spectral maximum, $\max\{S(f)\}$, had similar values from buoy and radar estimations in 55% of the cases and in 45% remaining cases the maximum of buoy spectra were higher than those of radar spectra. Fig. 7 shows the time series of $\max\{S(f)\}$ of buoy and radar spectra. It can be seen in the graphics of Fig. 7, values from buoy and radar show the largest differences during the range [26, 49] of data points. However, in this period the spectra from both sensors were very similar having different spectral maximum because the form of the radar spectra are smoother than those of buoy, as can be observed in the scalar spectrum of Fig. 3.

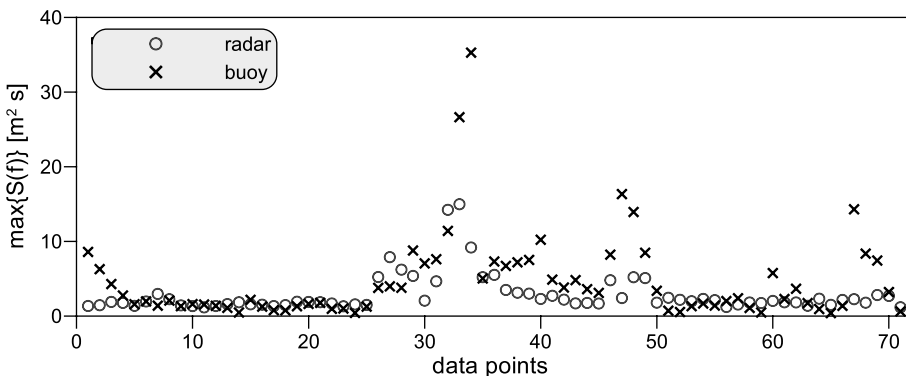


Fig. 7. Values of spectral maximum estimated from radar and buoy spectra.

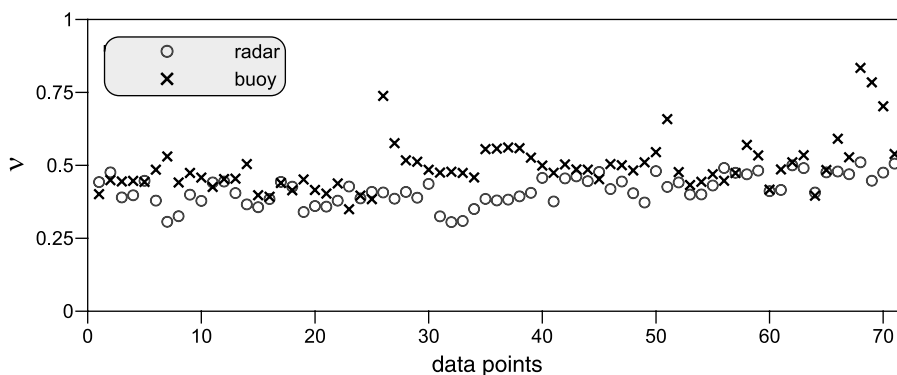


Fig. 8. Values of spectral bandwidth estimated from radar and buoy spectra.

6.5. Spectral bandwidth

The spectral bandwidth, ν , had values in mean similar from buoy and radar estimations as can be seen in the statistics of Tables 1 and 2. In Fig. 8, the values of this parameter estimated from radar and buoy are represented. It can be observed in the time series that the values of spectral bandwidth were around 0.4 from radar estimations, with all spectra being of narrow bandwidth, and 0.5 from buoy estimations, with 20% of these spectra having wide bandwidth. This parameter depends on the spectral moments of zero, first and second order and, as explained for the mean period, the moments of order greater than zero augment the weight of energy at higher frequencies. For this reason, the differences in the bandwidth resulted from energy of the buoy spectra located at frequencies higher than the maximum frequency of the radar spectra.

6.6. Mean direction

The values of mean direction, θ , were between northwest and southwest, corresponding to swells coming from these range of directions at the coastal line. The values of this parameter estimated from buoy and radar spectra are shown in the Fig. 8. In most of the cases, the estimations of buoy spectra were from northwest while the ones by radar spectra were from west, the radar presenting a deviation close to 25° southward with respect to buoy estimations. These discrepancies are due to diffraction on the coastal line. The radar measures at a zone closer to the coastal line (Fig. 1) where the Cape of Sines filters the waves coming from north and the buoy is located more to the south, so that it may register wave fields with less coastal effects. This fact was confirmed in cases were both sensors measured mean directions from southeast when this divergence disappeared, corresponding to range [26, 34] of data points (Fig. 9).

Fig. 10 shows two examples of the directional spectra and the mean direction in function of the frequency corresponding, respectively to the range of data points [26, 34] (Fig. 10(a)) and to the rest of the data points (Fig. 10(b)). The first is an example of the cases in which the estimated mean direction was similar from both sensors just

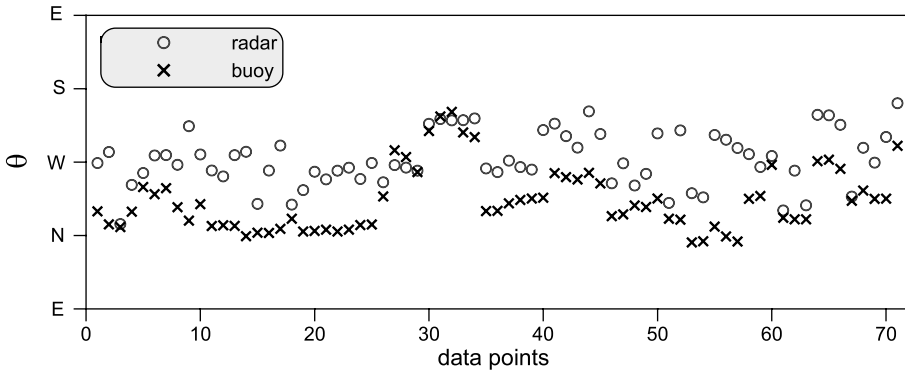


Fig. 9. Values of mean direction estimated from radar and buoy spectra.

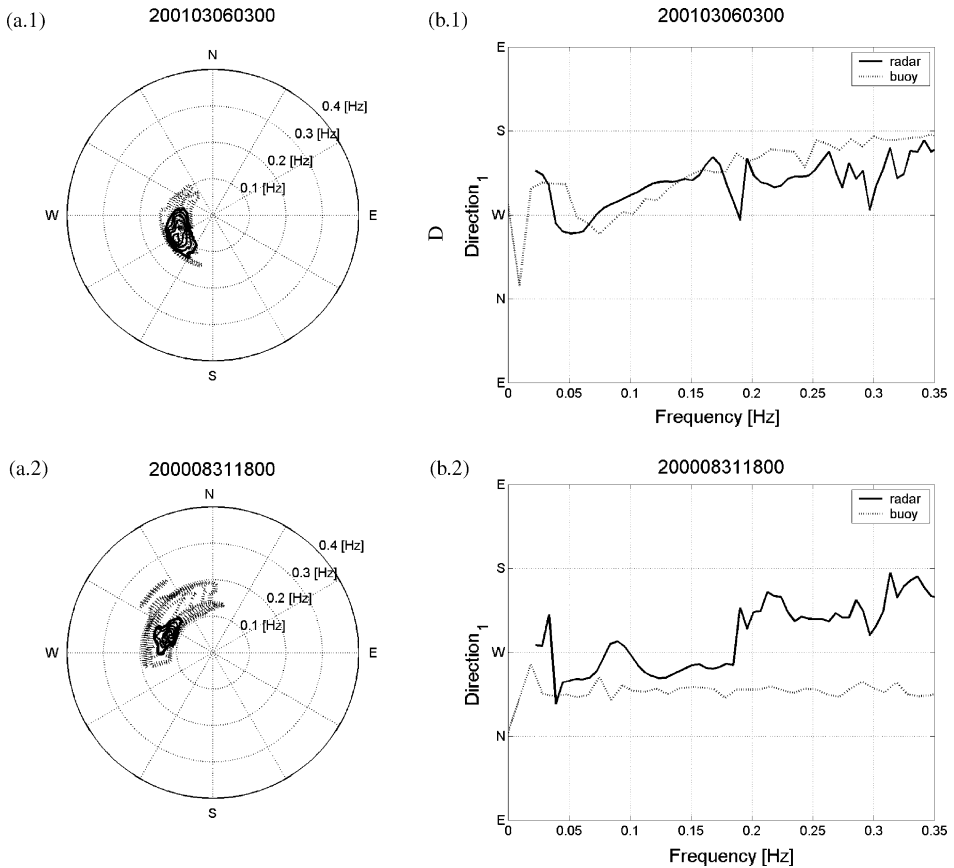


Fig. 10. Directional spectra from the radar (continuous line) and the buoy (dashed line) corresponding to the range of data points [26, 34], (a.1), and to the rest of data points, (a.2); and their respective mean direction in frequency, (b.1) and (b.2).

Table 3
Results of linear fit by least square from values of wind speed and noise level for each interval of azimuth degree

Degree interval	Number of points	<i>a</i>	<i>b</i>	R-squared	Minimum wind speed (m/s)	Wind speed mean (m/s)	rms
160–170	15	−34.42	23.97	0.8273	1.4	12.07	3.92
170–180	28	−30.46	23.38	0.8775	1.3	12.08	5.02
180–190	63	47.45	19.83	0.6688	2.4	10.12	4.54
190–200	46	−67.69	29.51	0.6345	2.3	5.90	2.41
200–210	19	−47.85	38.46	0.2778	1.2	3.97	1.31
210–220	15	−38.20	35.00	0.1942	1.1	4.35	1.49
220–230	16	27.36	17.15	0.3934	1.6	3.51	1.43
230–240	8	−26.46	29.31	0.7852	0.9	3.25	1.20
240–250	8	−158.31	70.34	0.9404	2.2	4.85	2.44
250–260	4	–	–	–	–	–	–
260–270	3	–	–	–	–	–	–
270–280	8	−20.82	16.36	0.5772	1.3	3.59	1.03
280–290	19	−189.10	60.40	0.2506	3.1	4.74	0.72
290–300	13	−42.53	29.43	0.4740	1.5	3.74	1.93
300–310	12	−118.90	59.09	0.8114	2.0	4.32	2.33
310–320	41	−99.29	52.84	0.8946	1.9	7.09	2.86

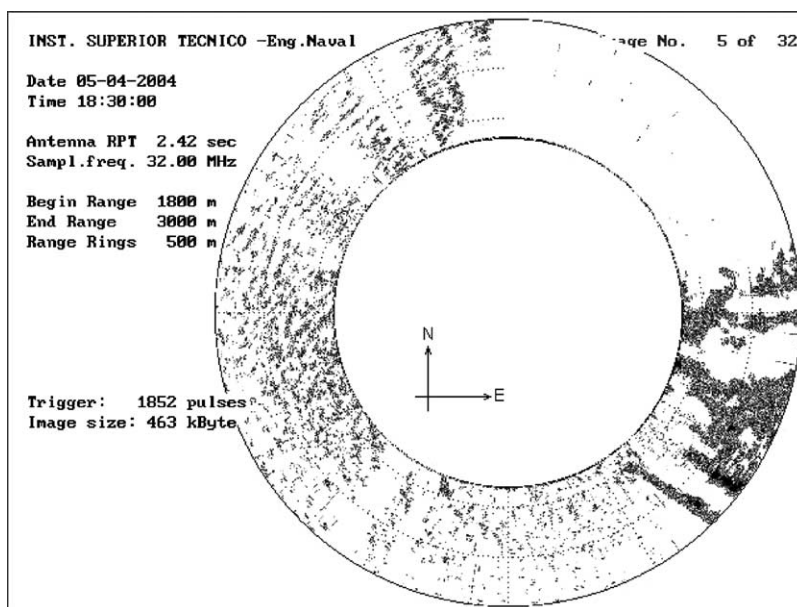


Fig. 11. An example of a polar image from radar of Sines.

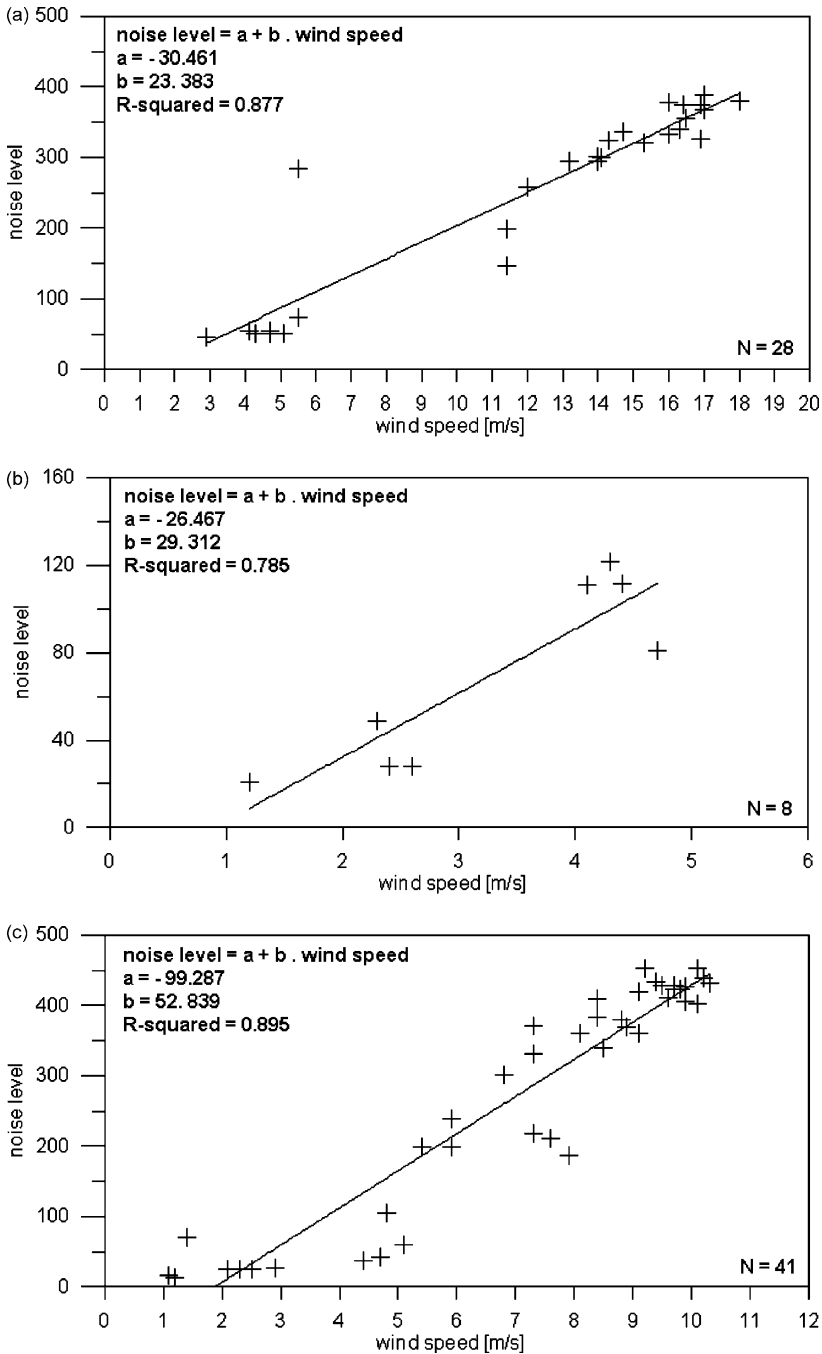


Fig. 12. A example of least-square fit to obtain the calibration parameters, a and b , of the Sines' radar, to calibrate the azimuth interval between 170–180, (a) 230–240, (b) 310–320, (c) degrees.

the directional spectra, in (a.1), and the mean direction in function of the frequency, in (b.1). The second is an example of most of the cases in which the directional spectra estimate from the buoy is located northward with respect to the radar spectra, graphic (a.2), and also the mean direction in function of the frequency, graphic (b.2), this behaviour is most noted with increasing frequency.

7. Wind speed

A data set of 925 simultaneous measurements of image time sequences, from the radar and wind speed and direction from the meteorological station, was used. The data set was grouped into 36 angle classes of 10° of azimuth to calibrate the radar in each interval. The azimuth is defined here as the angle between north direction and the antenna look direction being 0, 90, 180 and 270° , respectively North, East, South and West. For the calibration, it was assumed that the noise level of the image series is linearly related to the wind speed (Hatten et al., 1998) then a linear regression was made with those values for each angle class of azimuth.

Only the angle classes which had more than four simultaneous measurements from the radar and from the meteorological station were used in the linear regression for calibration. In Table 3 are presented the results of calibration for the directional intervals for which there is no land, i.e. between 160 and 330° as can be seen in the example of polar image of Fig. 11. In Table 3 is shown, for each class of angular directions, the values and the number of data used for the regression, the calibration parameters a and b , and the regression coefficient R -squared resulting of the linear fit. An example of the values of the noise level, from radar images, and the wind speed, from meteorological station, used in the calibration, is shown in Fig. 12 where the coefficients resulting of the linear fit for azimuth directions between 310 and 320° can be seen.

In this study of the performance of this radar to measure wind fields, not all directional intervals could be calibrated because there were some intervals which did not have enough wind measurements to make a linear fit according to the criteria. But it can be shown that for the other direction intervals the assumption of dependence of the spectral noise on the wind speed is approximated by a straight line. It can also be seen that the minimum speed of the wind that can be measured for this radar is in average 2 m per second for all degree intervals of directions.

8. Conclusions

In this paper a spectral analysis of the ocean waves and wind by the Sines' radar, as well as their calibration to estimate wave and wind fields has been presented. The scalar and directional spectra and several sea-state parameters, were compared with those estimated from a directional buoy situated near the area covered by the radar. The radar was calibrated using a meteorological station to measure wind for different directional sectors.

Spectral analysis was applied to measurements obtained from the radar and the buoy. The shape of the scalar spectra from radar data was smoother than that estimated from

buoy data because radar spectra contain spatial and temporal information while buoy spectra only contain temporal information. In the high frequency domain, the estimations performed by buoy were more adequate because the frequency resolution of the buoy is larger. In directional domain the radar provided spectra with less dispersion because the buoy data has less directional resolution. Due to the different location of the areas in which the measurements were made, the directional spectra from radar data had more directions southward than those from buoy data.

The significant wave height, peak frequency and spectral bandwidth estimated by both sensors had in general similar values. The bias that resulted from the mean period was identified as resulting from lack of appropriate description of the high frequencies in the radar data. In more cases, the spectral maximum from buoy spectra had higher values because the radar spectra have smoother shape. There is a bias in the mean direction attributed to the slightly different location of buoy and radar covered area, having the last one some shadow for the Cape of Sines.

In this work, it can be seen general good agreement with the estimations from the buoy and the spread is not too large. However, the present system had limitations in frequency resolution, which in revealed at high frequencies because the radar has a too large antenna rotation period. This results from having adopted the existing traffic control radar which characteristics were limited to wave monitoring as a large rotation period of the antenna.

The calibration of this radar to measure the wind speed showed a good agreement for the directional sectors that the wind is coming from sea. The value minimum to the wind speed detected for this radar was in mean 2 m per second and the values for the different degree intervals were between 0.9 and 3.1 m per second.

Acknowledgements

This work has been performed within the RADSEANET project (EUREKA-EUROMAR E1893) that was financed in Portugal by Agência de Inovação in the IC-PME/III/S program (contract no. L0085). The data were collected by Administração do Porto de Sines (APS).

References

- Alfonso, M., Munoyerro, A., Nieto Borge, J.C., 1997. Directional wave navigation radar measurements compared with pitch-roll buoy data. *Journal of Offshore Mechanics and Arctic Engineering* 119, 25–29.
- Alpers, W., Hasselmann, K., 1982. Spectral signal to clutter and thermal noise properties of ocean wave imaging synthetic aperture radars. *International Journal of Remote Sensing* 3, 423–446.
- Dankert, H., Horstmann, J., Koch, W., Rosenthal, W., 2002. Ocean wind fields retrieved from radar-image sequences, Proceedings of the International Geosciences and Remote Sensing Symposium, June 24–28, Toronto, Canada.
- Hatten, H., Ziemer, F., Seemann, J., Nieto Borge, J.C., 1998a. Correlation between the spectral background noise of a nautical radar and the wind vector. Proceedings of Seventeenth International Conference on Offshore Mechanics and Arctic Engineering, OMAE98-4451.

- Hatten, H., Seemann, J., Horsmann, J., Ziemer, F., 1998b. Azimuthal dependence of the radar cross section and the spectral background noise of a nautical radar at grazing incidence, Proceedings of IGARS'98 Conference, Seattle, USA.
- Heathershaw, A.D., Blackley, M.W.L., Hardcastle, P.J., 1980. Wave directional estimates using in coastal waters using radar. *Coastal Engineering* 3, 249–267.
- IAHR working group on wave generation and analysis, 1989. List of sea state parameters. *Journal of Waterway, Port, Coastal and Ocean Engineering* 37, 235–257.
- Izquierdo, P., Guedes Soares, C., Fontes, J.B., 2002. Monitoring of waves with X-band radar in the port of Sines, In: Dahlin, H., Fleming, N.C., Nittis, K., Petersson, S.E. (Eds.), *Building the European Capacity in Operational Oceanography*. Elsevier, Amsterdam, pp. 154–160.
- Izquierdo, P., Guedes Soares, C., Nieto Borge, J.C., Rodríguez, G.R., 2004. A comparison of sea state parameters from nautical radar images and buoy data. *Ocean Engineering*, 31, 2209–2225.
- Longuet-Higgins, M.S., Cartwright, D.E., Smith, N.D., 1963. Observations of the directional spectrum of sea waves using motions of floating buoy. *Proceedings of Conference Ocean Wave Spectra*, 111–132.
- Nieto Borge, J.C., Guedes Soares, C., 2000. Analysis of directional wave fields using X-band navigation radar. *Coastal Engineering* 40, 375–391.
- Nieto Borge, J.C., Reichert, K., Dittmer, J., 1999. Use of nautical radar as a wave monitoring instrument. *Coastal Engineering* 37, 331–342.
- Seemann, J., Ziemer, F., Senet, C.M., 1997. A method for computing calibrated ocean wave spectra from measurements with a nautical X-band radar, *Proceedings of Oceans'97 Conference*, Halifax, Canada, vol. 2, pp. 1148–1154.
- Senet, C.M., Seemann, J., Ziemer, F., 1997. Current and wave observation from coastal and vessel mounted stations by marine radar, *Proceedings of the Fourth International Conference on Remote Sensing for the Marine and Coastal Environments*, Orlando, pp. I,485–I,491.
- Young, I.R., Rosenthal, W., Ziemer, F., 1985. A three-dimensional analysis of marine radar images for the determination of ocean wave directionality and surface currents. *Journal of Geophysical Research* 90 (C1), 1049–1059.